J. Fluid Mech. (2006), *vol.* 564, *pp.* 267–285.
doi:10.1017/S0022112006001467 Printed in the United Kingdom

Roughness effects in turbulent pipe flow

By M. A. SHOCKLING[1], J. J. ALLEN[2] AND A. J. SMITS[1]

[1]Department of Mechanical and Aerospace Engineering, Princeton University, Princeton NJ 08540, USA

[2]Department of Mechanical Engineering, New Mexico State University, Las Cruces, NM 88046, USA

(Received 20 April 2005 and in revised form 27 March 2006)

Mean flow measurements are presented for fully developed turbulent pipe flow over a Reynolds number range of 57×10^3 to 21×10^6 where the flow exhibits hydraulically smooth, transitionally rough, and fully rough behaviours. The surface of the pipe was prepared with a honing tool, typical of many engineering applications, achieving a ratio of characteristic roughness height to pipe diameter of 1 : 17000. Results for the friction factor show that in the transitionally rough regime this surface follows a Nikuradse (1933)-type inflectional relationship rather than the monotonic Colebrook (1939) relationship used in the Moody diagram. This result supports previous suggestions that the Moody diagram in the transitional regime must be used with caution. Outer scaling of the mean velocity data shows excellent collapse and strong evidence for Townsend's outer layer similarity hypothesis for rough-walled flows. Finally, the pipe exhibited smooth behaviour for scaled roughness height $k_s^+ \leqslant 3.5$, which supports the suggestion by Zagarola & Smits (1998) that their pipe was hydraulically smooth for $Re_D \leqslant 24 \times 10^6$.

1. Introduction

The general behaviour of turbulent pipe flow in the presence of surface roughness is well established. For a given surface finish, the roughness is often described in terms of a characteristic roughness height k. This characteristic height may be taken as the root-mean-square roughness height k_{rms}, or the 'equivalent sandgrain roughness' height k_s defined by Nikuradse (1933). When k is small compared to the pipe diameter D, the flow behaviour changes with increasing Reynolds number. At low Reynolds numbers, the flow is smooth (there is no effect of roughness). As the Reynolds number increases, the flow becomes transitionally rough (the friction factor rises above the smooth value and is a function of both roughness height and Reynolds number), and eventually becomes fully rough (where the friction factor is independent of Reynolds number). In terms of the viscous length scale ν/u_τ (where $u_\tau \equiv \sqrt{\tau_w/\rho}$, ν is the fluid kinematic viscosity, τ_w is the wall shear stress, and ρ is the fluid density), the flow is smooth when $k^+ = ku_\tau/\nu$ is small, and fully rough when k^+ is so large that viscosity is no longer important. In the fully rough regime, the wall shear varies quadratically with the velocity, implying that form drag on the roughness elements is the principal source of the streamwise pressure drop.

With respect to the velocity profile, roughness disrupts the viscous sublayer and causes the non-dimensional velocity U/u_τ in the overlap region, commonly identified with a logarithmic velocity distribution, to shift down without changing its slope. At sufficiently high Reynolds numbers, or large enough relative roughness ϵ $(= k/D)$, the

velocity becomes independent of viscosity, although it retains its logarithmic distribution. In the outer region of the flow, it is expected that roughness manifests itself only in terms of a changing wall stress, so that the velocity profile in outer layer coordinates is unaffected by roughness, assuming, of course, that k remains small compared to D. This is known as Townsend's (1976) hypothesis of outer layer similarity.

Interest in the effects of roughness on wall-bounded turbulence is being driven by a number of recent developments. Krogstad & Antonia (1999) noted that symptoms of roughness can be measured in the outer flow, which would invalidate Townsend's hypothesis. Flack, Schultz & Shapiro (2005) suggested that the roughness elements used by Krogstad & Antonia (1999) were a significant fraction of the boundary layer thickness, which may have influenced their results. The work of Flack *et al.* (2005) shows a universal collapse in the outer layer, even though their largest non-dimensional roughness height was significantly larger than that used by Krogstad & Antonia (1999). Jiménez (2004) makes the point that experiments with both a large k^+ and a small $\epsilon = k/D$ (or k/δ, where δ is the 99 % thickness) are required to resolve these apparent contradictions.

The question of when roughness effects first become important was discussed by Perry, Hafez & Chong (2001), McKeon *et al.* (2004) and McKeon, Zagarola & Smits (2005). This discussion hinges on the influence of roughness in the transitional regime, an issue that has been the subject of controversy since the work of Nikuradse (1933) was first published. It also touches on how the characteristic roughness height can be determined for an arbitrary roughness distribution, and whether a single length scale is an adequate description.

Here, we describe experiments in a honed pipe with $k_{rms}/D = 19.4 \times 10^{-6}$, over a range of Reynolds numbers from 57×10^3 to 21.2×10^6, where k_s^+ varies from 0.17 to 44.4. The honed surface finish was chosen because of its industrial importance, and also because the results can be compared to those obtained by Zagarola & Smits (1998) and McKeon *et al.* (2004) for a similar surface finish with $k_{rms}/D = 1.16 \times 10^{-6}$. The results presented here are the first to show the entire progression from smooth to fully rough behaviour for an extremely small value of k_{rms}/D.

2. Flow scaling

In terms of the skin friction, we expect that

$$\tau_w = \phi(\overline{U}, D, \nu, \rho, k) \tag{2.1}$$

where $\overline{U}$ is the average or bulk velocity, and ϕ denotes a functional dependence. For a pipe flow, therefore, the friction factor λ varies according to

$$\lambda = \phi_1(Re_D, k/D) \tag{2.2}$$

or, equivalently,

$$\lambda = \phi_2(Re_D, k^+) \tag{2.3}$$

where $\lambda \equiv 8\tau_w/(\rho\overline{U}^2)$, and $Re_D = \overline{U}D/\nu$. Note that for fully developed flow, $4\tau_w/D = -\mathrm{d}p/\mathrm{d}x$, where $\mathrm{d}p/\mathrm{d}x$ is the streamwise pressure gradient. There is no universal friction factor curve for rough pipe flow, but for smooth pipes McKeon *et al.* (2005) found that the curve

$$\frac{1}{\sqrt{\lambda}} = 1.930\,\log(Re_D\sqrt{\lambda}) - 0.537 \tag{2.4}$$

fits pipe flow data for $31 \times 10^3 \leqslant Re_D \leqslant 35 \times 10^6$ to within 1.25 %.

In terms of the mean velocity distribution for negligible roughness, we start with the usual distinction between the inner and outer layers, where for the inner layer

$$U = f_1(y, u_\tau, \nu, R) \tag{2.5}$$

and for the outer layer

$$U_{CL} - U = g_1(y, u_o, \nu, R) \tag{2.6}$$

where U is the mean velocity, U_{CL} is the centreline velocity, R is the pipe radius ($D = 2R$), and u_o is the outer layer velocity scale (as defined by Zagarola & Smits 1998). Hence,

$$\frac{U}{u_\tau} = f_2(y^+, R^+) \tag{2.7}$$

and

$$\frac{U_{CL} - U}{u_\tau} = g_2(\eta, R^+) \tag{2.8}$$

where $y^+ = yu_\tau/\nu$, $R^+ = Ru_\tau/\nu$, and $\eta = y/R$. If we confine our attention to Reynolds numbers sufficiently high such that the inner and outer scales are independent of R^+, then

$$U^+ = f(y^+) \tag{2.9}$$

for the inner flow, where $U^+ = U/u_\tau$, and

$$U^+_{CL} - U^+ = g(\eta) \tag{2.10}$$

for the outer flow. Under these conditions, complete similarity in Reynolds number applies. Millikan (1938) proposed that, for $\nu/u_\tau \ll y \ll R$, an overlap between the inner and outer regions may exist, where by matching the velocity gradient we obtain for the inner layer:

$$U^+ = \frac{1}{\kappa} \ln y^+ + B \tag{2.11}$$

and for the outer layer:

$$U^+_{CL} - U^+ = -\frac{1}{\kappa} \ln \eta + B^*. \tag{2.12}$$

According to McKeon *et al.* (2004), von Kármán's constant $\kappa = 0.421 \pm 0.002$, $B = 5.60 \pm 0.08$, and $B^* = 1.20 \pm 0.1$.

With increasing Reynolds number and a fixed pipe diameter, the viscous length scale ν/u_τ decreases relative to D and may become comparable to the characteristic roughness height, k. At this point, roughness will start to play a role in determining the flow characteristics. Under conditions of complete similarity, the inner layer scaling becomes

$$U^+ = f(y^+, k^+). \tag{2.13}$$

If we assume, as argued by Towsend (1976), that roughness only affects the outer layer scaling by modulating the wall stress (that is, by changing u_τ), then the outer layer formulation is independent of the direct effects of roughness and equation (2.10) continues to hold for rough wall flows. The overlap argument in this transitionally rough regime gives

$$U^+ = \frac{1}{\kappa} \ln y^+ + B - \Delta U^+ \tag{2.14}$$

where ΔU^+ is Hama's (1954) roughness function that depends only on k^+. With further increases in Reynolds number, or if the roughness height is made larger, a

point will be reached where the inner scaling no longer depends on viscosity, and

$$U^+ = f\left(\frac{y}{k}\right). \tag{2.15}$$

The overlap argument in this fully rough regime gives

$$U^+ = \frac{1}{\kappa}\ln\frac{y}{k} + B'. \tag{2.16}$$

Here, B' is called the Nikuradse roughness function, and it is expected to be constant when the flow is fully rough. From equations (2.14) and (2.16), we see that in the fully rough regime the Hama roughness function behaves according to

$$\Delta U^+ = \frac{1}{\kappa}\ln k^+ + B - B'. \tag{2.17}$$

Since the wall shear stress in the fully rough regime is a function of the square of the velocity, it is often assumed that the flow resistance in the pipe is akin to a form drag. Bradshaw (2000), however, notes that the concept of a critical roughness height for the onset of roughness may be erroneous, and that the data of Nikuradse (1933) for the size of the velocity shift could equally support a power-law departure starting at zero roughness. Bradshaw also notes that standing eddies form behind objects at about the same Reynolds number as the critical roughness value. However, the presence of standing eddies does not cause a sudden change in the drag coefficient. In addition, the departure from Stokes drag occurs for a roughness Reynolds number of the order of unity, and if the drag over sparsely spaced elements follows an Oseen expansion, the variation of the velocity shift B' should be proportional to k^2 when $k^+ > 1$.

3. Roughness functions

For a given roughness type, the behaviour in the transitional roughness regime is known only from experiment. For a surface consisting of closely packed, nearly mono-disperse sandgrain roughness, Nikuradse (1933) found that the flow was smooth for $k_s^+ \leqslant 5$, transitionally rough for $5 < k_s^+ < 70$, and fully rough for $k_s^+ \geqslant 70$. Here, $k_s^+ = k_s u_\tau/\nu$, and k_s was taken to be the average sandgrain height. Many other types of roughness have been studied, and the behaviour in the transitional region can vary widely (see, for example, figure 3 of Jiménez 2004).

Part of the difficulty in comparing roughness functions in the transitionally rough regime is that the roughness height k is not well defined. Indeed, it seems obvious that an arbitrary surface will need more than one characteristic scale to describe its effect on the near-wall flow. Nevertheless, in order to compare different types of surfaces, it is usual to prescribe an equivalent sandgrain roughness that relates k_{rms} for a given surface to a particular sandgrain roughness height k_s. The equivalent sandgrain roughness is found by comparing the friction factor of the surface in question with Nikuradse's sandgrain data in the fully rough regime, independent of the particular form of the roughness function in the transitional rough regime. As an example, Hama (1954) suggests that for a machined surface with an approximately Gaussian distribution of roughness elements the equivalent sandgrain roughness is $k_s \simeq 5k_{rms}$. Similarly, Zagarola & Smits (1998) suggested that for a honed and polished surface, $k_s \simeq 3k_{rms}$.

We have noted that the roughness functions for different surfaces can vary widely. Surfaces such as those investigated by Nikuradse (1933), the mesh roughness investigated by Perry & Abell (1977), and the tightly packed spheres studied by Ligrani & Moffat (1986), all display friction factor curves that show an inflection point, in that the friction factor is higher than the smooth pipe value at the same

Reynolds number but falls below the fully rough value before rising to meet it. We will describe this type of roughness function as 'inflectional', where it is recognized that different roughness geometries can produce varying strengths of inflection. In contrast, the roughness function proposed by Colebrook (1939) to describe the transitional roughness behaviour of industrial surfaces approaches the fully rough friction factor value from above. We will describe this type of roughness function as 'monotonic'. The differences in friction factor between inflectional and monotonic behaviour at the same Reynolds number may depend on the ratio of roughness height to boundary layer thickness, k/δ. For the studies showing inflectional roughness this ratio is typically very small, but for the studies showing monotonic roughness it can be as high as 5%.

On the basis of laboratory experiments on rough pipes performed by Colebrook & White (1937), and a large collection of friction factor data obtained from pipes in commercial use, Colebrook (1939) proposed the following transition function to describe the friction factor between the hydraulically smooth and fully rough regimes:

$$\frac{1}{\sqrt{\lambda}} = -2\log\left(\frac{k_s}{3.71D} + \frac{2.51}{Re_D\sqrt{\lambda}}\right). \tag{3.1}$$

The equivalent sandgrain roughness for each surface was found by estimating the friction factor in the fully rough regime (this process sometimes required extrapolation since the data in the fully rough regime were not always available). Colebrook's roughness function satisfies two asymptotic conditions: one that it approaches Prandtl's smooth pipe friction factor curve as $k_s^+ \to 0$, and the other that Nikuradse's fully rough behaviour is approached as $k_s^+ \to \infty$. It is this roughness function that is used in the Moody diagram (Moody 1944), and Perry *et al.* (2001) assumed that honed pipes (as studied by Zagarola & Smits 1998 and McKeon *et al.* 2004) followed this monotonic roughness behaviour.

Hama (1954) conducted a study of rough wall turbulent boundary layers with an eventual goal of "... being able to predict the resistance for any combination of flow and roughness characteristics". Hama found that the roughness functions of his simulated 'natural roughness' behaved like inflectional rather than monotonic Colebrook-type roughness. The problem of poor correlation of experimental data with the Colebrook curves is not new, as the discussion section of Moody (1944) makes clear.

Zagarola & Smits (1998) performed experiments in nominally smooth pipe flow at Reynolds numbers from 31×10^3 to 35×10^6. However, Perry *et al.* (2001) raised the possibility that roughness affected these 'Superpipe' experiments for Reynolds numbers greater than about $Re_D = 400 \times 10^3$. In contrast, Zagarola & Smits (1998), by inspection of their values of ΔU^+, suggested that roughness did not become important for $Re_D \leqslant 24 \times 10^6$. McKeon & Smits (2002) and McKeon *et al.* (2003) showed that, although Zagarola & Smits (1998) had used an inaccurate correction on the static pressure, the pipe was, by all criteria, smooth up to a Reynolds number of at least 13.6×10^6. Nevertheless, the work of Perry *et al.* (2001) draws into the spotlight the use and validity of the Colebrook functions to describe transitionally rough flows, in this case for a honed and polished surface.

4. Experiment

The Princeton University/ONR Superpipe facility was used for all experiments. This turbulent pipe flow facility uses compressed air at pressures up to 200 atm as the working fluid to achieve Reynolds numbers from 31×10^3 to 35×10^6, as shown in figure 1 and described in detail by Zagarola (1996) and Zagarola & Smits (1998).

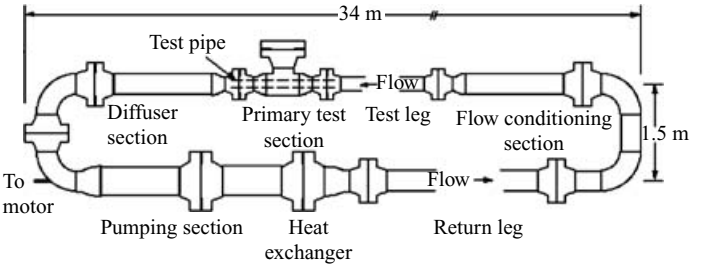

FIGURE 1. Princeton/ONR Superpipe facility.

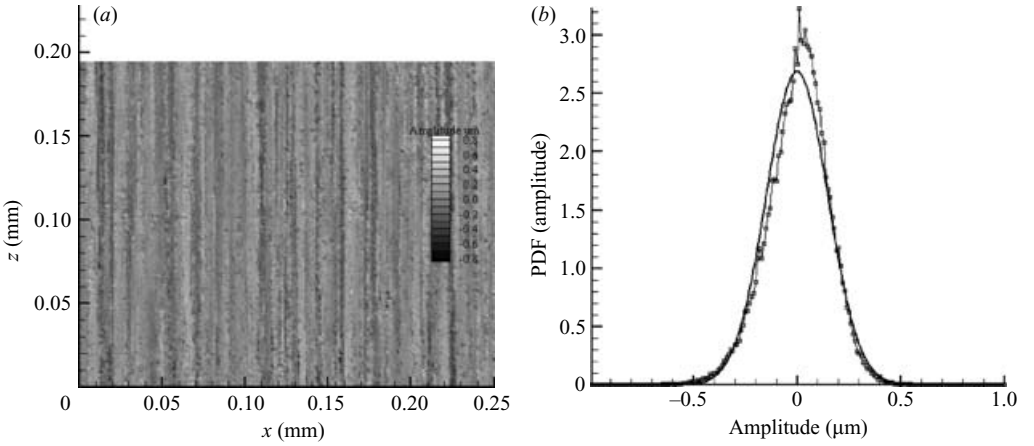

FIGURE 2. (*a*) Two-dimensional surface plot of the original Superpipe. Area shown is about 0.2 mm × 0.25 mm, and the amplitudes are in μm. (*b*) Probability density function of surface elevation.

The test pipe is located inside the closed-return pressure vessel, and it is approximately 0.129 m in diameter and 25.9 m in length, so that the length-to-diameter ratio exceeds 200. Two test ports are available at $160D$ and $196D$ downstream of the contraction, and all profiles were measured at the downstream location during these experiments. The pipe was constructed using 5 in. (129 mm) ID, 1/2 in. (12.7 mm) thick drawn aluminum tube. Six sections of tube, approximately 4.6 m in length, were connected and the centreline axis was aligned to within ± 1.25 mm over a distance of 30 m using the alignment procedure described by Zagarola (1996). Since the pipe sections were connected during honing, the maximum step measured at each joint during installation was about ± 0.025 mm over the entire length of the pipe, negligibly small according to Zagarola (1996).

The pipe surface roughness was designed to be geometrically similar to the surface used by Zagarola & Smits (1998) and McKeon *et al.* (2004) while preserving a low k_{rms}/D. A machined surface roughness is typically described using the roughness and r.m.s. amplitudes, defined respectively as $R_a = \int_0^L |y/L|\,\mathrm{d}x$, and $R_q = (\int_0^L (y/L)^2\,\mathrm{d}x)^{1/2}$, where y is the surface height deviation from the mean level. For the original Superpipe surface, comparator plates indicated that $R_a \approx 0.15$ μm. To better define the geometry of the surface roughness, a non-interfering, two-dimensional optical measurement was made of the original Superpipe surface, as shown in figure 2. From this image, it is

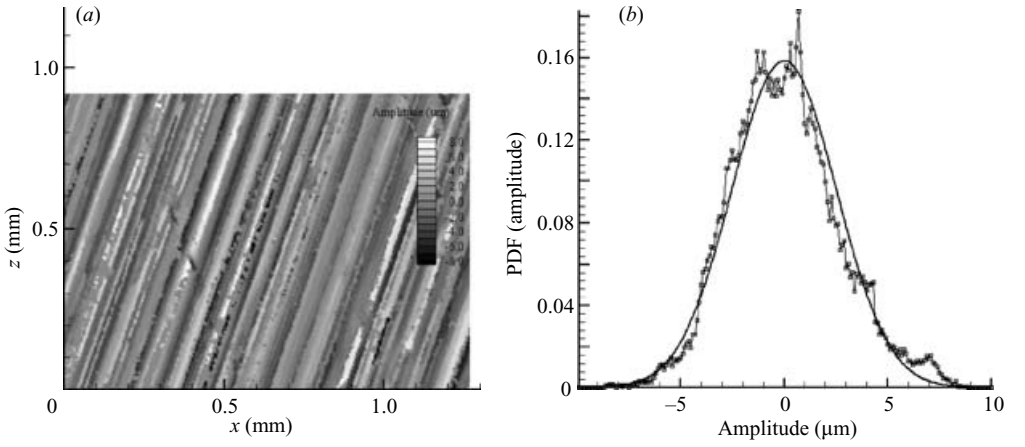

FIGURE 3. (*a*) Two-dimensional surface plot of the new rough pipe. Area shown is about 0.8 mm × 1.2 mm, and the amplitudes are in μm. (*b*) Probability density function of surface elevation.

clear that a particular wavelength has been imparted to the surface as a result of the honing process. However, it can also be seen that the probability density function of the surface elevation closely resembles a normal distribution, with a skewness of only −0.31, and a flatness of 3.6. The data give $R_a = 0.116\,\mu\text{m}$ and $R_q = 0.15\,\mu\text{m}$, in good agreement with the original comparator plate measurements.

One other useful measure that is relevant to the pipe surface design is the high spot count (HSC), which is the number of peaks per unit length that exceed a certain threshold. Using a threshold value for the peak counts equal to R_q results in a mean wavelength, defined as $\lambda_{HSC} = 1/HSC$ of 0.01 mm. Therefore the ratio of roughness height to wavelength was very small in the original Superpipe experiments ($\simeq 1/62$), and raises the question as to whether traditional concepts such as form drag behind discrete objects can be used to describe the flow field over such a surface.

The new rough pipe was designed using the Colebrook roughness function so that the flow was expected to be smooth up to $Re_D \simeq 500 \times 10^3$, and fully rough for $Re_D > 8 \times 10^6$. A surface with an equivalent sandgrain roughness value of $k_s = 7.6\,\mu\text{m}$ appeared to satisfy these requirements. Using $k_s \simeq 3k_{rms}$, as suggested by Zagarola & Smits (1998), gives $k_{rms} = 2.5\,\mu\text{m}$, and the new pipe was honed to obtain this roughness and an appropriately scaled λ_{HSC}.

Figure 3 shows a two-dimensional plot of the surface elevation, generated using an optical scanner of the new surface. For this surface, $R_q = 2.5\,\mu\text{m}$ and $R_a = 1.92\,\mu\text{m}$. The surface skewness was $Sk = 0.31$ and the flatness was 3.43. Again, these results suggest that the roughness distribution is close to being Gaussian. Using a threshold value for the peak counts equal to R_q gives $\lambda_{HSC} = 90\,\mu\text{m}$, and an amplitude-to-wavelength ratio of $\simeq 1/37$. Although the rough surface is not geometrically identical to the original Superpipe smooth surface, it is expected that the roughness scaling for this surface will reflect closely the behaviour of the smooth Superpipe at equivalent k_s^+ conditions since both surfaces show nearly Gaussian roughness distributions.

5. Measurement techniques

Mean velocity profiles were taken $196D$ downstream of the test pipe inlet. A removable oval shaped plug, 100 mm × 50 mm wide was inserted into the test pipe,

to which the probe traverse assembly was attached. The interior surface of the plug formed a smooth fit with the pipe surface, and the plug was in place during honing, ensuring surface continuity. Two Pitot probes similar in design to those of Zagarola & Smits (1998) were used for the velocity profile measurement, with diameters of 0.64 mm and 0.43 mm. The probes were tested against a United Sensor standard probe in a large atmospheric wind tunnel, demonstrating agreement within 0.2 %. Two 0.40 mm static pressure taps were located on the plug surface to serve as the reference pressure for all measurements. The velocity profile consisted of 48 points, spaced logarithmically. Sampling time of the differential pressure signals was 90 s at 50 Hz for each point in the velocity profile. Five points were taken past the centreline to demonstrate flow symmetry. Twenty-one 0.79 mm diameter static pressure taps, spaced 165.1 mm apart, were used to determine the pressure gradient. An Acurite linear encoder provided probe location measurements with a resolution of $\pm 5\,\mu$m. Forward and reverse travel of the probe, a total distance of about 150 mm, was achieved with a repeatability within 25 μm (less than 4 % of the larger Pitot probe diameter).

Owing to the large range of differential pressures encountered in the experiment, several pressure transducers were used. For the tests at atmospheric pressure, MKS Baratron transducers were used and placed external to the pressure vessel. These 1 Torr and 10 Torr transducers had an uncertainty of ± 0.2 % full scale. For the pressurized tests, Validyne DP-15 strain-gauge transducers were used and were located inside the pressure vessel. The ranges of these sensors were 0.2 p.s.i.d. (1380 Pa), 1.25 p.s.i.d. (8600 Pa), 5 p.s.i.d. (34 500 Pa), and 12 p.s.i.d. (83 000 Pa). All of the Validyne transducers were accurate to ± 0.5 % of full scale and calibrated against industry standards. Temperature readings in the pressure vessel were taken using a standard Chromel–Alumel thermocouple interfaced with an Omega DP-41-TC-AR indicator, accurate to ± 0.1 %. The ambient pressure for the atmospheric tests was recorded using a mercury manometer, accurate to ± 35 Pa. When the pipe was pressurized, the internal pressure P_{abs} was measured with one of two sensors. At pressures below 3.4 atm (3.4×10^5 Pa), an Omega transducer calibrated to an accuracy of ± 350 Pa was used, and for the higher pressure tests, up to 170 atm (17×10^6 Pa), a Heise pressure gauge was used, accurate to ± 3500 Pa. A PC equipped with a National Instruments BNC-2110 DAC card was used to collect data and control the experiment, which was fully automated with LabVIEW software. The typical duration for an experiment was 2.5 h, including the 21-point pressure gradient measurement and 48-point velocity profile, with appropriate settling time between points. Air temperature in the pipe during an experiment was kept constant to within ± 0.6 K.

6. Data analysis

To deduce the velocity from measurements using a Pitot probe and a wall static pressure tap, a number of corrections need to be made. These corrections are due to the effects of viscosity, turbulence level, velocity gradient, presence of a wall, and viscous effects on the static tap reading. For a full description of the correction techniques see Chue (1975) and McKeon *et al.* (2003).

The effects due to the presence of a velocity gradient were dominated by the displacement of the streamlines, and the data were corrected using the method suggested by McKeon *et al.* (2003), where the apparent position of a probe of diameter d is displaced away from the wall by an amount $\Delta y/d$ according to a local non-dimensional velocity gradient

$$\alpha = \frac{\mathrm{d}U}{\mathrm{d}y}\frac{d}{2U}, \tag{6.1}$$

such that $\Delta y/d = 0.15\tanh(4\sqrt{\alpha})$. This relationship approaches that of MacMillan (1956) for large velocity gradients, where $\Delta y/d = 0.15$, and has the advantage over the MacMillan correction that it does not apply a correction when there is zero shear.

As the probe approaches the surface, the extent of the streamline displacement will depend not only on the local shear but also on the presence of the wall. Corrections for this effect were applied using the displacement correlations proposed by McKeon & Smits (2002) for $y/d < 2$, where

$$\frac{\delta_w}{d} = \begin{cases} 0.150, & d^+ < 8, \\ 0.120, & 8 < d^+ < 110, \\ 0.085, & 110 < d^+ < 160. \end{cases} \tag{6.2}$$

The correction was applied such that $y_c = y + \delta_w$, where y_c is the corrected location associated with the velocity measurement.

In general, the pressure measured using a static tap will tend to overestimate the actual static pressure at the wall since the flow over the static tap will be deflected into the pressure tapping hole. The magnitude of this error depends primarily on the static port Reynolds number. McKeon *et al.* (2003) conducted an extensive series of tests and showed that, in contrast to the findings of Shaw (1960), the error continues to increase with Reynolds number. The corrections proposed by McKeon *et al.* (2003) were used to correct all data presented here.

For the present experiment, differences between the correction method of MacMillan (1956) and McKeon *et al.* (2003) were within experimental uncertainty, and the use of a MacMillan correction as opposed to that used here does not influence the behaviour shown in § 7.

Perry *et al.* (2001) interpreted the original smooth Superpipe data with additional turbulence corrections based on measurements of Perry, Henbest & Chong (1986), Abell (1974), and Durst, Jovanovic & Sender (1995). Such a correction requires an accurate turbulence intensity profile, which is not known for this surface. Without adequate information to appropriately correct for turbulence intensity, we present here the data only corrected for Pitot and static tap error. Also, it is expected that the turbulence intensity correction is much smaller than the Pitot and static tap corrections. Zagarola & Smits (1998) reported corrections typically on the order of 0.3 % of the local velocity for high-Reynolds-number experiments and a maximum correction less than 0.6 %, which occurred at low Reynolds number.

An additional source of uncertainty in the static pressure tap reading comes from roughness effects very near the tap. Based on the static pressure taps used to determine the axial pressure drop in this pipe, the uncertainty in any individual static tap was approximately ± 0.2 % at the highest Reynolds number of $Re_D = 21.2 \times 10^6$ (see Shockling 2005).

A direct test of these correction techniques comes from the ability to collapse data using different size Pitot probes onto the same velocity profile. Figure 4 shows a comparison between the two probes (0.64 mm and 0.43 mm), for four different tests in the smooth regime, in the range $68 \times 10^3 \leqslant Re_D \leqslant 116 \times 10^3$, after the application of the shear corrections of McKeon *et al.* (2003) and the static correction of McKeon & Smits (2002). The agreement near the wall, where the corrections are most significant, is very satisfactory.

Sources of experimental uncertainty include estimating the pressure gradient from a linear fit to measurements of the wall pressure at 21 ports, finding the average or bulk velocity using a curve fit to the near-wall data to represent the velocity profile from $y = 0$ to the first data point, the uncertainty in determing the density and viscosity, and the uncertainty in each pressure transducer. The contributions to the total uncertainty

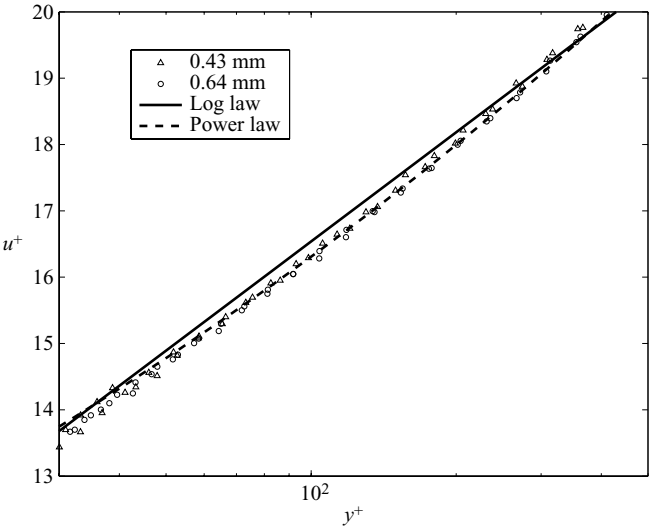

FIGURE 4. Corrected velocity profiles for two probe sizes, 0.64 mm and 0.43 mm, for $68 \times 10^3 \leqslant Re_D \leqslant 116 \times 10^3$. - - - -, $U^+ = 8.48 y^{+(0.142)}$; ——, $U^+ = (1/0.421) \ln y^+ + 5.60$.

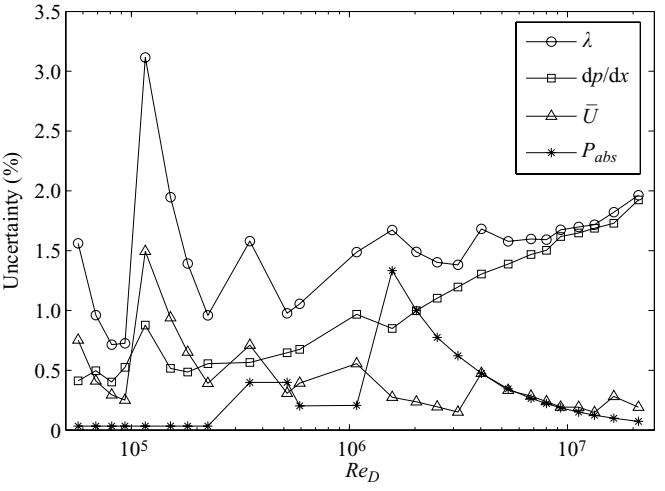

FIGURE 5. Uncertainty analysis for λ, $\mathrm{d}p/\mathrm{d}x$, $\bar{U}$ and P_{abs} as a function of Re_D.

in λ, $\mathrm{d}p/\mathrm{d}x$, $\bar{U}$, and P_{abs} are summarized in figure 5. The large increases in $\bar{U}$ and P_{abs} uncertainty occur when switching from one pressure transducer to another as the pressure in the facility is increased. A full uncertainty analysis is given in Shockling (2005).

7. Results

7.1. *Friction factor*

Figure 6 shows the friction factor in the pipe over the full range of Reynolds number. Note that error bars have only been shown on λ and not on Re_D, which shows negligible error on a semi-logarithmic plot. The data agree well with the smooth curve relationship of McKeon *et al.* (2005) (equation (2.4)) up to $Re_D \simeq 1.5 \times 10^6$, where the

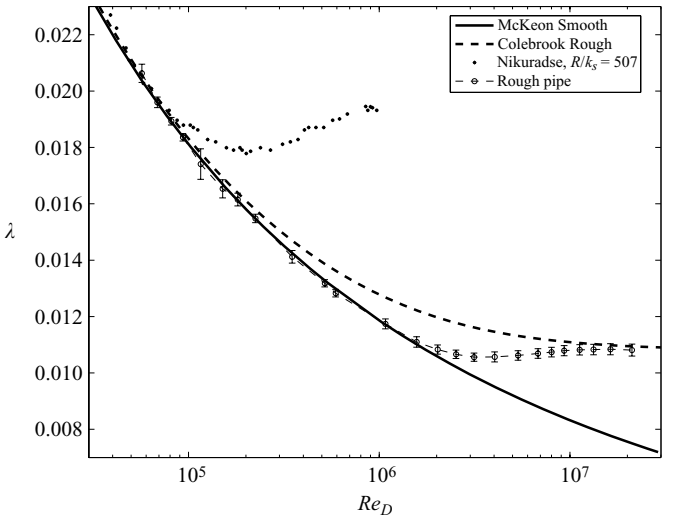

FIGURE 6. Friction factor λ for the present surface, compared with the rough-all relations of Colebrook (1939) for the same k_s, the smooth-wall relation of McKeon *et al.* (2005) (equation (2.4)), and the results for the smallest sandgrain roughness used by Nikuradse (1933).

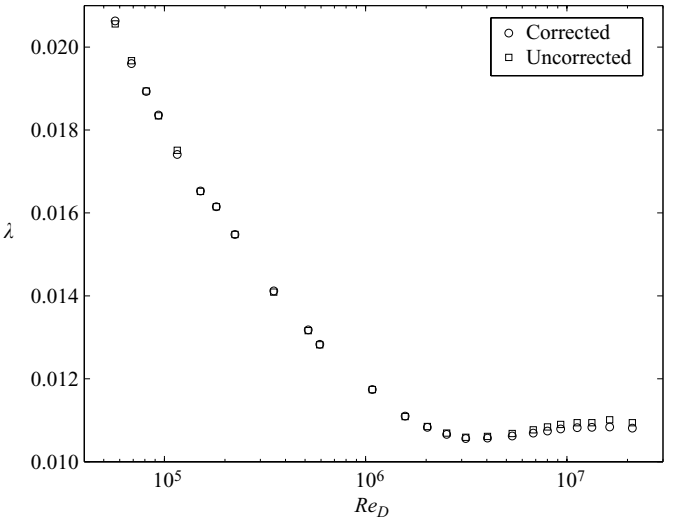

FIGURE 7. Friction factor λ for the present surface, comparing the data using corrections as described in § 6 and the data without any corrections.

friction factor begins to depart from the smooth curve, reaching a local minimum of $\lambda \simeq 0.0106$ in the region $3.1 \times 10^6 < Re_D < 4.0 \times 10^6$. The friction factor then rises to a constant value of $\lambda = 0.0108$ for $Re_D > 10 \times 10^6$. The equivalent sandgrain roughness for this surface, defined by the friction factor in the fully rough regime, is $k_s = 7.4\,\mu\text{m} = 3k_{rms}$, in good agreement with Zagarola & Smits's (1998) estimate $k_s \simeq 3k_{rms}$ for the smooth pipe data.

Figure 7 shows a comparison of the friction factor as calculated with the prescribed Pitot and static corrections to the friction factor without any corrections applied (for

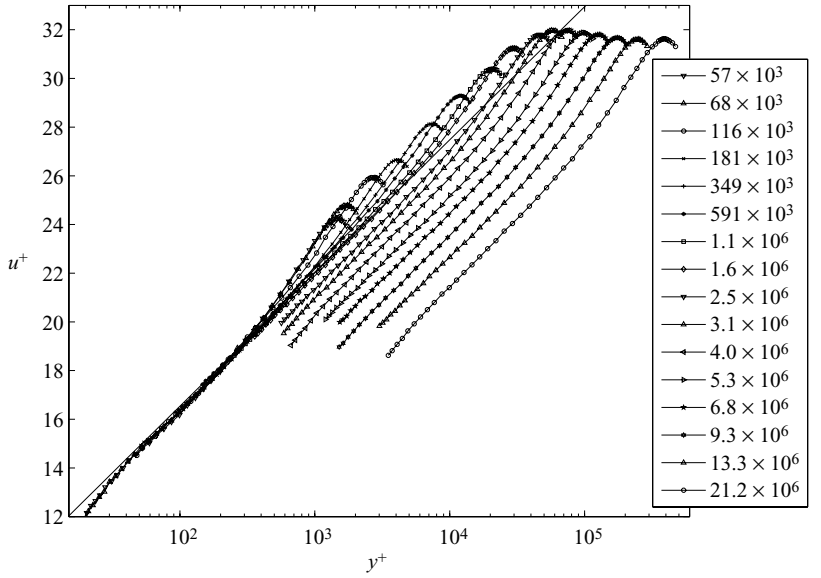

FIGURE 8. Velocity profiles over the full Reynolds number range. ——, $U^+ = (1/0.421)\ln y^+ + 5.60$.

a complete set of uncorrected and corrected data, see Shockling 2005, Appendices A and B). The maximum discrepancy between the two data sets is approximately 1.5%, occurring at $Re \simeq 16 \times 10^6$. The inflectional behaviour is effectively diminished by the applied corrections, and the difference between the corrected and uncorrected data sets is sufficiently small such that the inflectional phenomenon is beyond the magnitude of the correctional method. Since a turbulence intensity correction is expected to be smaller than the Pitot and static corrections, the inflectional behaviour remains.

The Colebrook curve corresponding to $k_s = 7.5\,\mu\text{m}$ is also shown in figure 6. Clearly, the Colebrook curve makes a poor prediction for the transitionally rough behaviour of this surface. At the point of departure from the smooth regime, at $Re_D \simeq 1.5 \times 10^6$, the Colebrook relation overestimates the friction factor by approximately 10%. The transitional regime is characterized by an inflectional curve, similar to the behaviour of the sandgrain roughness tested by Nikuradse (1933) and shown in figure 6 for $R/k_s = 507$. This result is somewhat unexpected because honed surfaces are often classified as natural or commercial roughness, and are therefore expected to follow a Colebrook, or monotonic, roughness behaviour as assumed by Perry *et al.* (2001).

7.2. *Velocity profile: inner scaling*

A more sensitive indicator for the effects of roughness is the behaviour of the velocity profiles. Figure 8 shows the velocity profiles for the entire Reynolds number range of the experiment. Figure 9 highlights the velocity profiles in the smooth regime; that is, where the friction factor lies on the smooth-wall correlation of McKeon *et al.* (2004) (equation (2.4)). This includes all data for $Re_D < 1.6 \times 10^6$. Zagarola & Smits (1998) and McKeon *et al.* (2004) found that the region $y^+ < 600$ was best described by a power law of the form $U^+ = 8.48y^{+(0.142)}$, and a similar phenomenon is seen here in that a small undershoot below the log law is seen near the wall. For $y^+ \geqslant 600$, the profiles show a region of logarithmic behaviour below the wake function, also in agreement with the earlier results of the smooth pipe. This is seen further in figure 10,

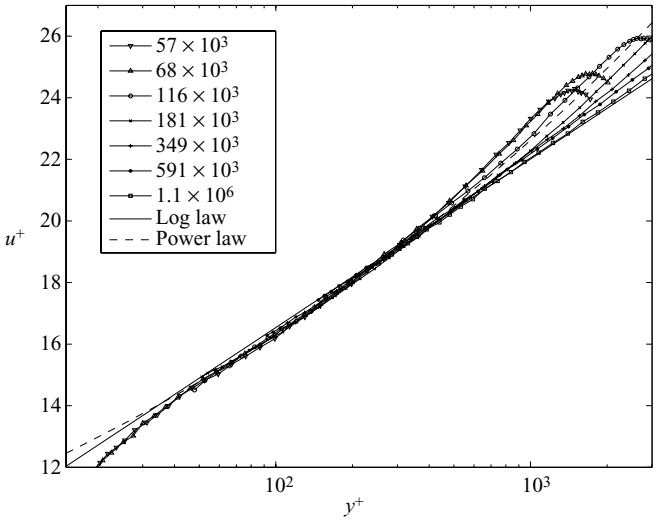

FIGURE 9. Velocity profiles in the smooth regime. - - - -, $U^+ = 8.48y^{+(0.142)}$; ——, $U^+ = (1/0.421)\ln y^+ + 5.60$.

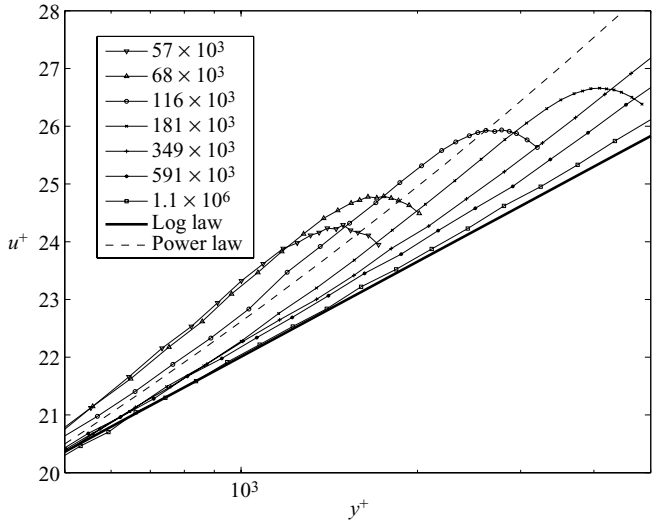

FIGURE 10. Velocity profiles in the smooth regime showing the logarithmic region and the wake function. - - - -, $U^+ = 8.48y^{+(0.142)}$; ——, $U^+ = (1/0.421)\ln y^+ + 5.60$.

although only one profile in the smooth regime was of high enough Reynolds number to demonstrate a significant region of logarithmic behaviour.

Figure 11 shows the velocity profiles in the transitional and fully rough regimes. The downward shift with increasing Reynolds number is as expected.

Zagarola & Smits (1998) and McKeon *et al.* (2005) calculated the value of κ by fitting the friction factor data such that

$$\frac{1}{\sqrt{\lambda}} = C_1 \log(Re_D\sqrt{\lambda}) + C_2, \tag{7.1}$$

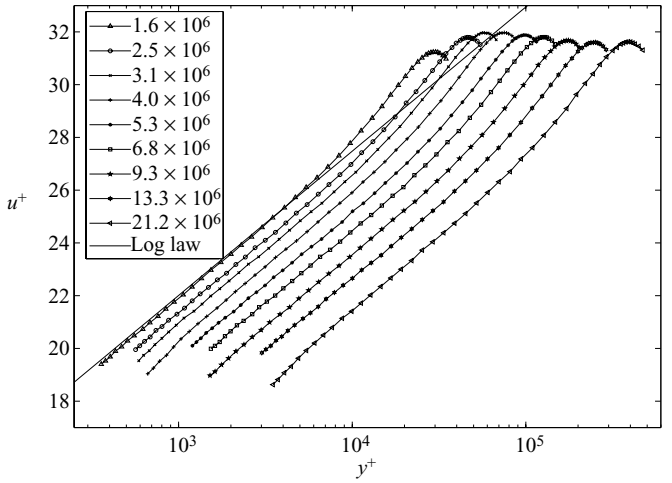

FIGURE 11. Velocity profiles in the transitional and fully rough regime. ——, $U^+ = (1/0.421)\ln y^+ + 5.60$.

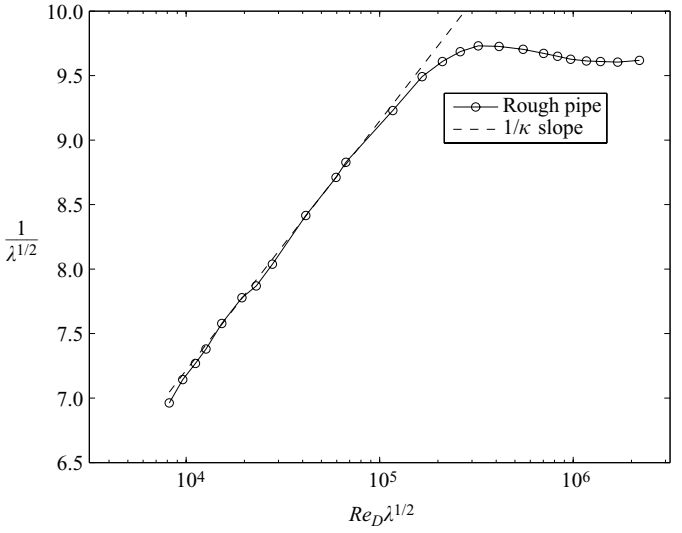

FIGURE 12. Friction factor relationship with Reynolds number as predicted by equation (7.1) in the smooth regime: ——, current data; - - - -, slope of $1/\kappa = 1/0.421$.

where

$$C_1 = \frac{1}{\kappa}\frac{1}{2\sqrt{2}\log(e)}. \tag{7.2}$$

This was shown to eliminate the variation in the log- law slope among individual experiments. For a rough pipe, κ cannot be found in the same way since λ rises above the smooth curve such that C_2 in equation (7.1) is no longer Reynolds number independent. Nonetheless, figure 12 shows the good agreement of the current hydraulically smooth data with the slope predicted by equation (7.1).

Shockling (2005) found κ and the value of $\psi = U^+ - 1/\kappa \ln y^+$ by a least-squares fit to the logarithmic region of each profile ($y^+ \geqslant \simeq 150$). Note that for a smooth

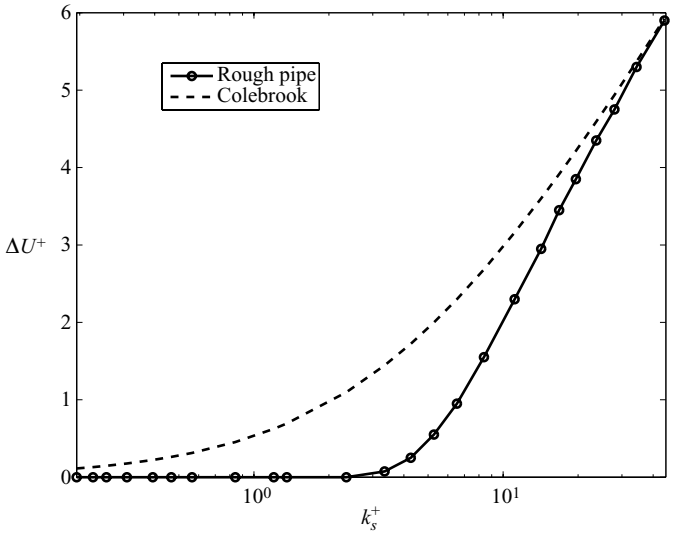

FIGURE 13. Hama roughness function. - - - -, Colebrook roughness function equation (3.1), with $k_s = 7.4 \times 10^{-6}\, m$; ——, ΔU^+ determined using McKeon's *et al.*'s (2004) constants.

surface, $\psi = B$, where B is the additive constant in the log law. The values for κ (at all Reynolds numbers) and ψ (in the smooth regime) agreed well with the values given by McKeon *et al.*, but the data are more scattered due to a higher level of experimental uncertainty in the presence of roughness.

The Hama roughness function is shown in figure 13 as a function of k_s^+. Here, ΔU^+ was determined by finding the best fit of the data to the log law, by fitting to the established log law given by McKeon *et al.* (2004) with the assumption that $\kappa = 0.421$ and $B = 5.6$. Here, the points in the transitional region follow a curve that more closely resembles the inflectional roughness of Nikuradse (1933) than the monotonic roughness of Colebrook (1939).

Perry *et al.* (2001) claimed that roughness effects were evident in the smooth Superpipe at values of k_s^+ as low as 0.05. This conclusion was based principally on the assumption that honed surface roughness displays a Colebrook-type transitional behaviour. The data presented here show that honed surface roughness does not deviate from hydraulically smooth conditions until $k_s^+ \simeq 3.5$, which occurs at a pipe Reynolds number that is about two orders of magnitude higher. The precise value of k_s for the original Superpipe experiment is unknown since the fully rough condition was not attained in that experiment. Nevertheless, an estimate can be made of the point of departure from smooth conditions by assuming that $k_s \simeq 3k_{rms}$ as found here for a geometrically similar surface. We find that the original Superpipe is expected to demonstrate hydraulically smooth behaviour for $Re_D \leqslant 27 \times 10^6$. By comparison, McKeon *et al.* (2004) analysed the velocity profiles to show that the Superpipe data were smooth, at a minimum, for $Re_D \leqslant 13.6 \times 10^6$. The original work by Zagarola & Smits (1998) suggested that the pipe was smooth up to Reynolds numbers of 24×10^6, in good agreement with the conclusion made here.

Figure 14 shows the velocity profiles shifted by the appropriate ΔU^+ from figure 13. With this shift applied, the profiles collapse onto the log law. Further evidence of this is seen in figure 15, in which the wake function, $y/R > \simeq 0.15$, has been removed

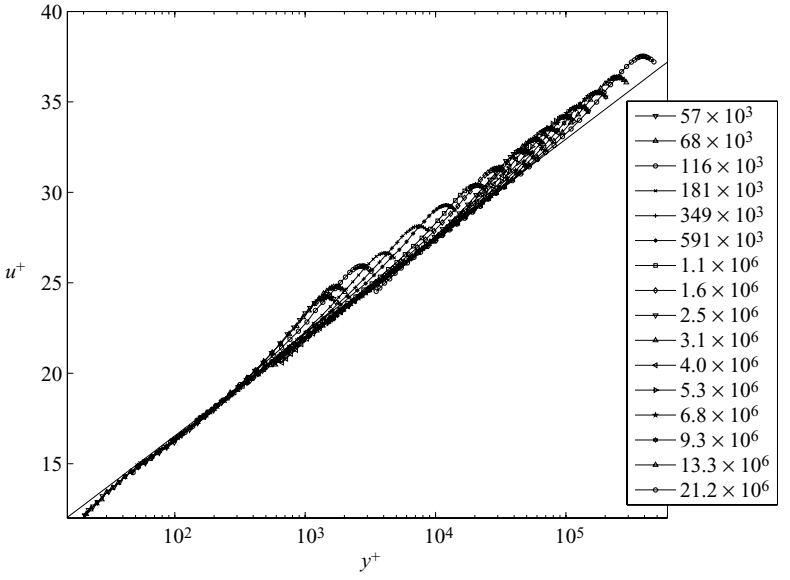

FIGURE 14. Velocity profiles shifted by the roughness function as given in figure 13. ——, $U^+ = (1/0.421)\ln y^+ + 5.60$.

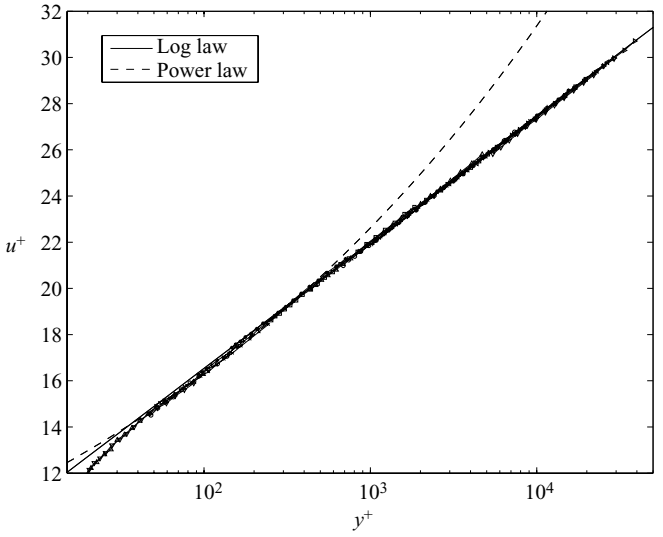

FIGURE 15. Velocity profiles shifted according to the values presented in figure 13. Wake functions have been removed to evaluate log law collapse. - - - -, $U^+ = 8.48y^{+(0.142)}$; ——, $U^+ = (1/0.421)\ln y^+ + 5.60$.

from the profiles. Agreement with the log law in the outer region, and the power law in the inner region, with the constants found by McKeon *et al.* (2004), is excellent.

Figure 16 shows the velocity shift in terms of the Nikuradse roughness function B', where $U^+ = (1/\kappa)\ln(y/k_s) + B'$. While the inflectional behaviour shown by the honed surface is not as pronounced as the sandgrain roughness of Nikuradse (1933) or tightly packed spheres of Ligrani & Moffat (1986), it clearly possesses a point of inflection. The current honed surface appears to reach fully rough conditions at a

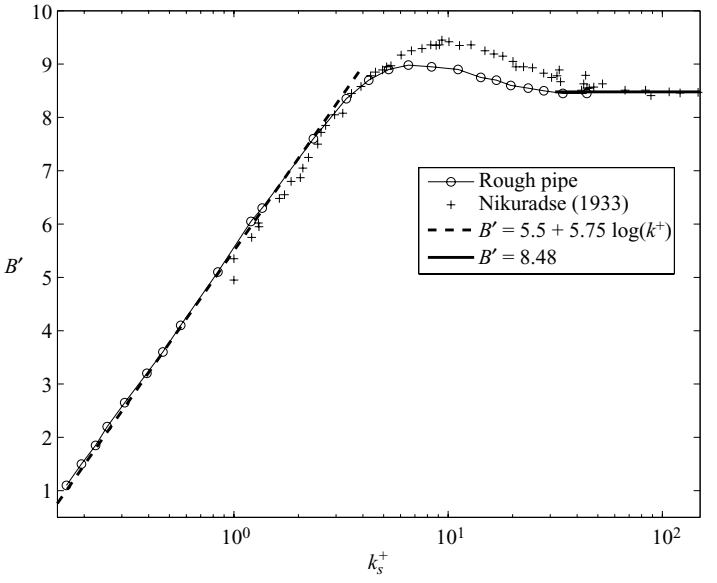

FIGURE 16. The velocity profile shift according to Nikuradse's roughness scaling, showing smooth, transitional, and fully rough regimes.

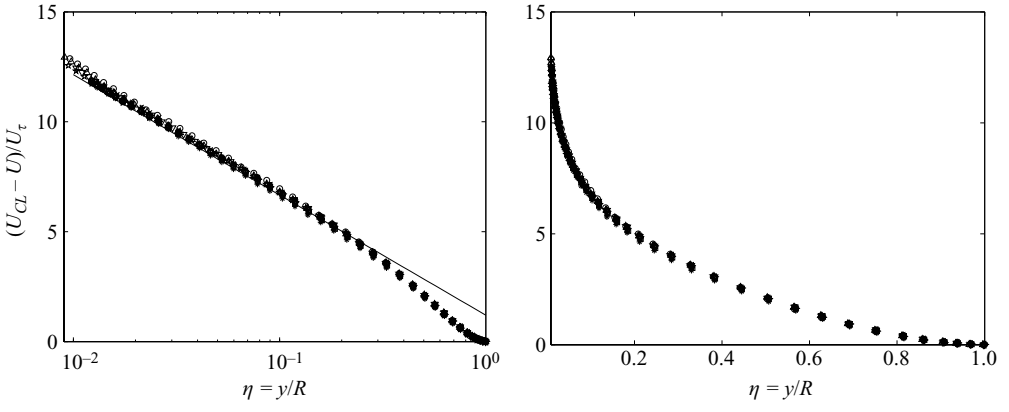

FIGURE 17. Outer scaling for $349 \times 10^3 \leqslant Re_D \leqslant 21.2 \times 10^6$. Solid line: $-(1/0.421)\ln\eta + 1.20$.

slightly lower roughness Reynolds number, k_s^+, which may be an effect of the random variation in surface elevation; honed roughness has a nearly Gaussian roughness distribution, whereas the roughness elements used by Ligrani & Moffat (1986) and Nikuradse (1933) had an extremely narrow bandwidth and would not necessarily possess a Gaussian distribution.

7.3. *Velocity profiles: outer scaling*

Figure 17 shows a collection of velocity profiles for $Re \geqslant 349 \times 10^3$ scaled on outer flow coordinates, y/R. It appears that the velocity profiles collapse well, as expected according to Townsend's outer flow similarity hypothesis for rough-wall flows. The collapse in outer layer coordinates is comparable to that demonstrated by Zagarola & Smits (1998) for the smooth Superpipe data and by Flack *et al.* (2005) in their rough-wall boundary layer studies.

7.4. *Moody diagram revision*

The inflectional transitional roughness behaviour of the current surface differs qualitatively from the monotonic transitional behaviour used in the Moody diagram, and a noticeable departure from hydraulically smooth conditions occurs at a relative roughness approximately two orders of magnitude larger than that predicted by the Moody diagram. For this reason, a revision is needed to better represent honed surfaces (and surfaces of similar geometry and industrial interest) with small relative roughness. A technique to calculate the resistance curve for a honed surface of arbitrary roughness height is detailed in Allen, Shockling & Smits (2005).

8. Conclusions

Honed surface roughness in fully developed turbulent pipe flow was investigated over the Reynolds number range $57 \times 10^3 \leqslant Re_D \leqslant 21.2 \times 10^6$, demonstrating hydraulically smooth, transitionally rough, and fully rough behaviour. The transitionally rough regime was found to follow the inflectional behaviour first observed by Nikuradse (1933) in pipes coated with sand grains of a narrow distribution of sizes. The friction factor did not follow the monotonic behaviour expressed by Colebrook's (1939) roughness function that forms the basis for the Moody diagram.

The equivalent sandgrain roughness of the surface was found to be $k_s \simeq 3k_{rms}$, in agreement with the suggestions of Zagarola & Smits (1998) for a surface produced by a similar honing process. The flow showed the first symptoms of roughness when $k_s^+ \approx 3.5$, contrary to the suggestions implicit in the Moody diagram and the arguments posed by Perry *et al.* (2001). It would appear that this is the critical roughness height for honed surfaces with $k \ll D$ (or $k \ll \delta$). On this basis, it is determined that the original smooth Superpipe exhibits hydraulically smooth behaviour for $Re_D \leqslant 27 \times 10^6$. For all conditions of roughness, logarithmic scaling was apparent at higher Reynolds numbers with the same constants determined by McKeon *et al.* (2004) for smooth pipes. An excellent collapse of the velocity profiles in outer scaling provides strong support for Townsend's hypothesis, at least for very small values of k_{rms}/D. The magnitude of the downward shift in the velocity profile, as measured by the Hama roughness function, was seen to follow transitional behaviour qualitatively similar to sandgrain roughness, again in contrast with Colebrook (1939).

The support of ONR under Grant No. N00014-03-1-0320, and NSF Grant No. CTS-9908442 is gratefully acknowledged. We also wish to thank Beverley McKeon for providing advice on correction methods, Mark Zagarola and Robert Bogart for advice on pipe design, Gary Kunkel for assistance with experimental techniques, and Jonathan Morrison for many useful discussions.

REFERENCES

Abell, C. J. 1974 Scaling laws for pipe flow turbulence. PhD thesis, University of Melbourne, Australia.

Allen, J. J., Shockling, M. A. & Smits, A. J. 2005 Evalution of a universal transition resistance diagram for pipes with honed surfaces. *Phys. Fluids* **17**, 121702.

Bradshaw, P. 2000 A note on "critical roughness height" and "transitional roughness". *Phys. Fluids* **12**, 1611–1614.

Chue, S. H. 1975 Pressure probes for fluid measurement. *Prog. Aerospace Sci.* **16**, 1–40.

Colebrook, C. F. 1939 Turbulent flow in pipes, with particular reference to the transitional region between smooth and rough wall laws. *J. Inst. Civ. Engng* **11**, 133–156.

Colebrook, C. F. & White, C. M. 1937 Experiments with fluid friction in roughened pipes. *Proc. R. Soc. Lond.* A **161**, 367–378.

Durst, F., Jovanovíc, J. & Sender, J. 1995 LDA measurements in the near-wall region of a turbulent pipe flow. *J. Fluid Mech.* **295**, 305–335.

Flack, K. A., Schultz, M. P. & Shapiro, T. A. 2005 Experimental support for Townsend's Reynolds number similarity hypothesis on rough walls. *Phys. Fluids* **17**, 035102.

Hama, F. R. 1954 Boundary-layer characteristics for smooth and rough surfaces.*Trans Soc. Naval Archit. Mar. Engrs* **62**, 333–358.

Jiménez, J. 2004 Turbulent flow over rough walls. *Annu. Rev. Fluid Mech.* **36**, 173–196.

Krogstad, P.-A. & Antonia, R. A. 1999 Surface roughness effects in turbulent boundary layers. *Exps. Fluids* **27**, 450–460.

Ligrani, P. M. & Moffat, R. J. 1986 Structure of transitionally rough and fully rough turbulent boundary layers. *J. Fluid Mech.* **162**, 69–98.

MacMillan, F. A. 1956 Experiments on Pitot-tubes in shear flow. *Aero. Res. Counc. R&M*. 3028.

McKeon, B. J., Li, J., Jiang, W., Morrison, J. F. & Smits, A. J. 2003 Pitot probe corrections in fully-developed turbulent pipe flow. *Meas. Sci. Tech.* **14**, 1449–1458.

McKeon, B. J., Li, J., Jiang, W., Morrison, J. F. & Smits, A. J. 2004 Further observations on the mean velocity distribution in fully developed pipe flow. *J. Fluid Mech.* **501**, 135–147.

McKeon, B. J. & Smits, A. J. 2002 Static pressure correction in high Reynolds number fully developed turbulent pipe flow. *Meas. Sci. Tech.* **13**, 1608–1614.

McKeon, B. J. Zagarola, M. V. & Smits, A. J. 2005 A new friction factor relationship for fully developed pipe flow. *J. Fluid Mech.* **538**, 429–443.

Millikan, C. M. 1938 A critical discussion of turbulent flows in channels and circular pipes. *Proc. 5th Intl Congr. Appl. Mech.* Wiley.

Moody, L. F. 1944 Friction factors for pipe flow. *Trans. ASME* **66**, 671–684.

Morrison, J. F., McKeon, B. J., Jiang, W. & Smits, A. J. 2004 Scaling of the streamwise velocity component in turbulent pipe flow. *J. Fluid Mech.* **508**, 99–131.

Nikuradse, J. 1933 Laws of flow in rough pipes. *VDI Forschungsheft* 361; also *NACA TM* 1292, 1950.

Perry, A. E. & Abell, C. J. 1977 Asymptotic similarity of turbulence structures in smooth and rough walled pipes. *J. Fluid Mech.* **79**, 785–799.

Perry, A. E., Hafez, S. & Chong, M. S . 2001 A possible reinterpretation of the Princeton superpipe data. *J. Fluid Mech.* **439**, 395–401.

Perry, A. E., Henbest, S. M. & Chong, M. S. 1986 A theoretical and experimental study of wall turbulence. *J. Fluid Mech.* **165**, 163–199.

Shaw, R. 1960 The influence of hole dimension on static pressure measurements. *J. Fluid Mech.* **7**, 550–564.

Shockling, M. A. 2005 Turbulent flow in a rough pipe. MSE Dissertation, Princeton University.

Streeter, V. L. 1935 Frictional resistance in artificially roughened pipes. *Trans. ASCE* **61**, 163–186.

Townsend, A. A. 1976 *The Structure of Turbulent Shear Flow*. Cambridge University Press.

Zagarola, M. V. 1996 Mean-flow scaling of turbulent pipe flow. Doctoral Dissertation, Princeton University.

Zagarola, M. V. & Smits, A. J. 1998 Mean-flow scaling of turbulent pipe flow. *J. Fluid Mech.* **373**, 33–79.